ISSN: 0067-2904

Numerical Simulation of Magnetohydrodynamic Influences on Casson Model for Blood Flow through an Overlapping Stenosed Artery

Ahmed Bakheet *[1], Esam A. Alnussairy[2]
[1] Department of Mathematics, College of Science, Mustansiriyah University, Baghdad, Iraq
[2] Department of Mathematics, College of Computer Science and Mathematics, Wasit University, Iraq.

Received: 19/8/2020 Accepted: 17/11/2020

Abstract

Magnetohydrodynamic (MHD) effects of unsteady blood flow on Casson fluid through an artery with overlapping stenosis were investigated. The nonlinear governing equations accompanied by the appropriate boundary conditions were discretized and solved based on a finite difference technique, using the pressure correction method with MAC algorithm. Moreover, blood flow characteristics, such as the velocity profile, pressure drop, wall shear stress, and patterns of streamlines, are presented graphically and inspected thoroughly for understanding the blood flow phenomena in the stenosed artery.

Keywords: Numerical simulation; Casson fluid; Pressure correction; overlapping stenosis.

محاكاة عددية لتأثير المغناطيسية الديناميكية على تدفق دم كاسون خلال الشريان الذي يعاني من تضيقات متداخل

احمد بخيت*[1]، عصام عبد الامير[2]
[1]قسم الرياضيات، كلية العلوم، جامعة المستنصريه، بغداد، العراق
[2]قسم الرياضيات، كلية علوم الحاسوب والرياضيات، جامعة واسط، واسط ، العراق

الخلاصة

تمت دراسة التأثيرات المغناطيسية الديناميكية لتدفق الدم غير المستقر على سائل كاسون عبر الشريان الذي يعاني من تضيقات متداخل. وقد تم تحديد المعادلات غير الخطية الحاكمة لتدفق الدم المصحوبة بالشروط الحدية المناسبة وحلها بناءً على تقنية الفروق المحدودة باستخدام طريقة تصحيح الضغط مع خوارزمية ماك. خصائص تدفق الدم مثل ملف تعريف السرعة ، وانخفاض الضغط ، وإجهاد قص الجدار وأنماط انسيابية الدم قدمت بشكل بياني وتم فحصها بدقة لفهم ظاهرة تدفق الدم في الشريان المريض.

1. Introduction

Stenosis is an abnormal increase in the thickness of the arterial wall that can develop at various locations in the vascular system under diseased conditions [1]. It can form in irregular shapes or as multiple or overlapping stenosis [2, 3]. Chakravarty and Mandal [4] stated that the presence of an overlapping stenosis in the artery is more critical than of a mild one. For this reason, researches have shown an increased interest to evaluate the effects of this kind of stenoses with different conditions and methods. An earlier study [4], extended by a later work [5], investigated the effects of on blood

*Email: ahmedbakheet@uomustansiriyah.edu.iq

flow characteristics. Both studies introduced blood as a Newtonian fluid. In addition, another work [6] examined the hemodynamics of the stenosed artery. To better understand this disease, an analytical study of blood flow considering the pressure variation along the axis of the artery was introduced [7]. The Newtonian model of blood was further considered [8, 9] to establish the impacts of the overlapping stenotic artery on the features of the flow. Also, this problem was adopted with steady equations and one-dimensional laminar blood flow [10], while another investigation [11] focused on the narrow artery and Casson fluid model. Furthermore, Ismail *et al.* [12] characterized blood flow as the generalized power law of fluids to determine the possible effects of tapered overlapping stenosis on streaming blood. COMSOL was employed to investigate the impacts of slip and magnetic field on power law model of blood flow [13]. The influences on blood flow properties were investigated using mild stenosis [14, 15]. Moreover, the effects of temperature and chemical reactions in the streaming blood through the tapered stenosed artery were studied and a Newtonian model of blood flow through a bifurcated stenosed artery was developed [16]. To gain further understanding of the influences of the overlapping stenosis, different blood models were applied in various studies; For instance, Jeffrey model [17], Casson model [18], couple stress fluids [19], polar fluid model ([20, 21], two-layered model ([3, 9, 22-25], and Rabinowitsch fluid model [26]. However, all previous researches did not calculate pressure drop and most of them involved velocities and wall shear only.

In this paper, Casson model of blood flow through an overlapping stenosis with the effects of MHD is considered. Blood flow was assumed to be unsteady and two-dimensional. A finite difference technique using the pressure correction method with marker and cell algorithm was employed to numerically solve the nonlinear governing equations.

2. Formation of the Governing Equations

Consider the blood flow through a uniform straight artery with an axisymmetric overlapping stenosis in a dimensionless form, as shown in Figure- 1 [7].

$$R(z)=\begin{cases}1-\dfrac{3\delta_x}{2L_0^4}\left[11(z-d)L_0^3-47(z-d)^2L_0^2+72(z-d)^3L_0-36(z-d)^4\right], & d\le z\le d+L_0\\ 1, \text{ otherwise}\end{cases} \tag{1}$$

where R (z) is the radius of the artery with stenosis, d indicates its location, and L_0, δ_x and r_c represent length, maximum height, and plug flow radius, respectively.

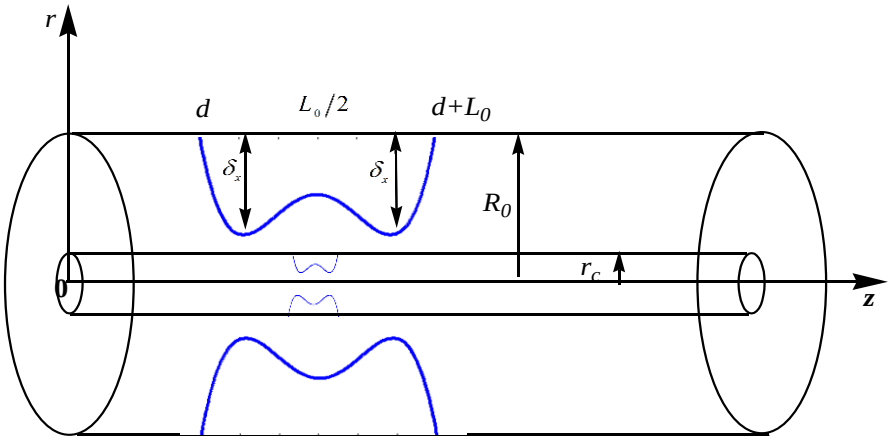

Figure 1- The geometry of the overlapping stenosis.

The governing equations of blood motion in the cylindrical polar coordinate system can be written in a conservative form as

$$\frac{\partial w}{\partial t}+\frac{\partial(wu)}{\partial r}+\frac{\partial w^2}{\partial z}+\frac{(wu)}{r}=-\frac{1}{\rho}\frac{\partial \mathrm{P}}{\partial z}-\frac{1}{\mathrm{Re}}\left[\frac{1}{r}\frac{\partial(r\tau_{rz})}{\partial r}+\frac{\partial(\tau_{zz})}{\partial z}+M^2w\right], \tag{2}$$

$$\frac{\partial u}{\partial t}+\frac{\partial u^2}{\partial r}+\frac{\partial(wu)}{\partial z}+\frac{u^2}{r}=-\frac{1}{\rho}\frac{\partial \mathrm{P}}{\partial r}-\frac{1}{\mathrm{Re}}\left[\frac{1}{r}\frac{\partial(r\tau_{rr})}{\partial r}+\frac{\partial(\tau_{rz})}{\partial z}\right], \tag{3}$$

$$\text{and}\qquad r\frac{\partial w}{\partial z}+\frac{\partial(ur)}{\partial r}=0, \tag{4}$$

where r and z are the radial and axial dimensionless coordinates scaled with respect to R_0. Meanwhile, the dimensionless w and u are scaled with respect to the cross-sectional average velocity U_0. Reynolds number Re, the dimensionless pressure P, the dimensionless shear stress τ_{ij}, and the Hartmann number M were defined as

$$\mathrm{Re}=\frac{\rho U_0 R_0}{\eta},\ \mathrm{P}=\frac{\mathrm{P}'}{\rho U_0^{\,2}},\ \tau_{ij}=\frac{\tau'_{ij}R_0}{\eta U_0},\ \text{and}\ M=R_0B_0\sqrt{\frac{\sigma}{\mu}}, \tag{5}$$

where the external magnetic field is B_0 and σ is the electrical conductivity.
While, the rheological equations of Casson fluid flow are given by Fung [27]

$$\tau_{zz}=-2\mu(J)\left(\frac{\partial w}{\partial z}\right), \tag{6}$$

$$\tau_{rr}=-2\mu(J)\left(\frac{\partial u}{\partial r}\right), \tag{7}$$

$$\tau_{rz}=-\mu(J)\left(\frac{\partial w}{\partial r}+\frac{\partial u}{\partial z}\right), \tag{8}$$

$$\text{with}\quad \mu(J)=\left[2^{-\frac{1}{2}}\tau_y^{\frac{1}{2}}+J^{\frac{1}{4}}\right]^2 J^{-\frac{1}{2}}, \tag{9}$$

$$\text{where}\quad J=\left[2\left\{\left(\frac{\partial w}{\partial z}\right)^2+\left(\frac{\partial u}{\partial r}\right)^2+\left(\frac{u}{r}\right)^2\right\}+\left(\frac{\partial w}{\partial r}+\frac{\partial u}{\partial z}\right)^2\right], \tag{10}$$

The model of Casson flow condition is given by

$$e_{ij}=\begin{cases}0 & \text{if}\quad J^*<\tau_y^2\\ \dfrac{1}{2\mu(J)}\tau_{ij} & \text{if}\quad J^*\geq\tau_y^2\end{cases}, \tag{11}$$

where $J^*=\frac{1}{2}\tau_{ij}\tau_{ij}$ is the stress tensor in the second invariant. $\mu(J)$, $J=\frac{1}{2}e_{ij}e_{ij}$, τ_y and η represent the apparent viscosity, strain tensor invariant rate, yield stress, and coefficient of viscosity, respectively.

Blood velocity boundaries of the arterial wall are no-slip [10]

$$w(r,z,t)=u(r,z,t)=0\quad \text{on}\ \ r=R(z), \tag{12}$$

and

$$\frac{\partial w(r,z,t)}{\partial r}=u(r,z,t)=0\ \text{on r = 0.} \tag{13}$$

For the Casson model, the inlet velocity conditions may be taken as described by Fung [25]

$$\begin{cases} w(r,0,t)=\left[\left(1-\left(\frac{r}{R}\right)^2\right)-\frac{8}{3}\sqrt{\frac{r_c}{R}}\left(1-\sqrt{\frac{r^3}{R^3}}\right)+2\frac{r_c}{R}\left(1-\frac{r}{R}\right)\right]U_0(t)\ \text{if}\ \ r_c\leq r<R(z),\\ w(r,0,t)=\left[(1-\frac{8}{3}\sqrt{\frac{r_c}{R}}+2\frac{r_c}{R}-\frac{1}{3}\left(\frac{r}{R}\right)^2)\right]U_0(t)\qquad \text{if}\ \ 0\leq r\leq r_c,\\ \text{and}\ \ u(r,0,t)=0, \end{cases} \tag{14}$$

and for inlet velocity we have $U_o(t)=\begin{cases}1, & \text{for steady velocity}\\ 1-\varepsilon_w\left[1+\cos(\omega t+\delta_o)\right], & \text{for pulsatile velocity,}\end{cases}$

with $U_o(0)=0$ and the angular frequency is ω. ε_w is an adjustable parameter which maintains the same stroke volume as a physiological flow waveform having the same stroke volume as the physiological flow. By using the condition $U_o(0)=0$, the value of $\delta_O=\cos^{-1}\left\{\frac{(1-\varepsilon_w)}{\varepsilon_w}\right\}$.

Conditions for the outlet velocities are given by

$$\frac{\partial w(r,z,t)}{\partial z}=0=\frac{\partial u(r,z,t)}{\partial z} \quad \text{at} \quad z=L \tag{15}$$

where the length of the artery is *L*. Furthermore, if it is supposed that there is no flow takes place as system is at rest except the flow at the inlet,

$$w(z,r,0)=0=u(r,z,0) \quad \text{and} \quad \mathrm{P}(r,z,0)=0 \quad \text{for } z>0. \tag{16}$$

3. Solution Development

For the purpose of avoiding interpolation error while discretizing the governing equations and to map the constricted domain into a rectangular one, the transformation $\zeta=\frac{r}{R(z)}$ was adopted.

Equations (2)-(4), (6)-(8), and (10) with the boundary conditions (12)-(16) become

$$\frac{\partial w}{\partial t}=-\frac{1}{R}\left[\frac{\partial(wu)}{\partial\zeta}-\zeta\frac{\partial \mathrm{P}}{\partial\zeta}\frac{dR}{dz}\right]-\frac{\partial w^2}{\partial z}+\frac{\zeta}{R}\frac{dR}{dz}\frac{\partial w^2}{\partial z}-\frac{wu}{\zeta R}-\frac{\partial \mathrm{P}}{\partial z}$$
$$-\frac{1}{\mathrm{Re}}\left[\frac{1}{R}\frac{\partial\tau_{\zeta z}}{\partial\zeta}+\frac{\tau_{zz}}{\zeta R}+\frac{\partial\tau_{zz}}{\partial z}-\frac{\zeta}{R}\frac{dR}{dz}\frac{\partial\tau_{zz}}{\partial\zeta}+M^2w\right] \tag{17}$$

$$\frac{\partial u}{\partial t}=-\frac{1}{R}\left[\frac{\partial u^2}{\partial\zeta}+\frac{\partial \mathrm{P}}{\partial\zeta}\right]-\frac{\partial(wu)}{\partial z}+\frac{\zeta}{R}\frac{dR}{dz}\frac{\partial(wu)}{\partial\zeta}-\frac{u^2}{\zeta R}$$
$$-\frac{1}{\mathrm{Re}}\left[\frac{1}{R}\frac{\partial\tau_{\zeta\zeta}}{\partial\zeta}+\frac{\tau_{\zeta\zeta}}{\zeta R}+\frac{\partial\tau_{\zeta\zeta}}{\partial z}-\frac{\zeta}{R}\frac{dR}{dz}\frac{\partial\tau_{\zeta\zeta}}{\partial\zeta}\right] \tag{18}$$

$$\zeta R\left[\frac{\partial w}{\partial z}-\frac{\zeta}{R}\frac{\partial w}{\partial\zeta}\frac{dR}{dz}\right]+\frac{\partial(\zeta u)}{\partial\zeta}=0, \tag{19}$$

$$\tau_{zz}=-2\mu(J_2)\left(\frac{\partial w}{\partial z}-\frac{\zeta}{R}\frac{\partial w}{\partial\zeta}\frac{dR}{dz}\right), \tag{20}$$

$$\tau_{\zeta\zeta}=-2\mu(J_2)\left(\frac{1}{R}\frac{\partial u}{\partial\zeta}\right), \tag{21}$$

$$w(\zeta,z,t)=u(\zeta,z,t)=0 \quad \text{at } \zeta=\mathrm{l}, \tag{22}$$

$$\frac{\partial w(\zeta,z,t)}{\partial\zeta}=\mathrm{u}(\zeta,z,t)=0 \text{ on } \zeta=0. \tag{23}$$

$$\begin{cases} w(\zeta,0,t)=U_o(t)\left[\left(1-\zeta^2\right)-\frac{8}{3}\sqrt{\zeta_c}\left(1-\zeta^{\frac{3}{2}}\right)-2\zeta_c\left(\zeta-1\right)\right], \text{ if } \quad \zeta_c\le\zeta<\mathrm{l}, \\ w(\zeta,0,t)=U_o(t)\left[\left(1-\frac{8}{3}\sqrt{\zeta_c}+2\zeta_c\left(1-\frac{\zeta_c}{6}\right)\right]\right. \qquad \text{if} \quad 0\le\zeta\le\zeta_c, \\ \text{and } u(\zeta,0,t)=0, \text{ where } \zeta_c=\frac{\tau_y}{2} \end{cases} \tag{24}$$

$$\frac{\partial w(\zeta,z,t)}{\partial z}=\frac{\partial u(\zeta,z,t)}{\partial z}=0 \text{ at } \quad z=L \tag{25}$$

$$w(\zeta,z,0)=u(\zeta,z,0)=\mathrm{P}(\zeta,z,0)=0 \quad \text{for } z>0. \tag{26}$$

4. Numerical Procedure

The equations were solved by the finite difference method in a uniform grid. $\zeta = j\,\Delta\zeta,\ z = i\,\Delta z,\ t = n\Delta t$ and $\mathrm{P}(\zeta, z, t) = \mathrm{P}(j\,\Delta\zeta, i\,\Delta z, n\Delta t) = \mathrm{P}^{n}_{i,j}$. Here, n refers to the time direction, Δt is the increment, and $\Delta\zeta, \Delta z$ are the length and width of the $(i, j)^n$ cell of the control volume, respectively, as shown in Figure-2.

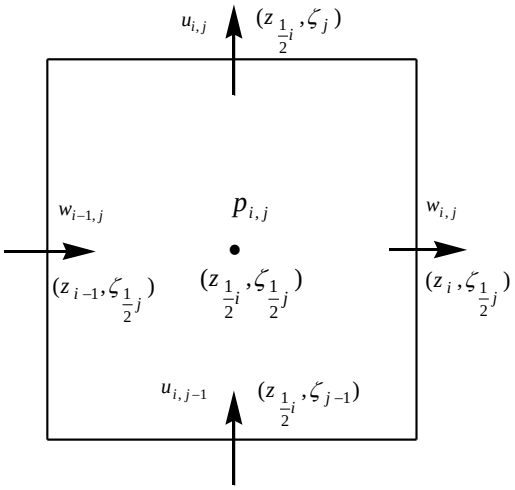

Figure 2-Typical MAC

Consequently, equation (19) was discretized by the second order accurate three point central difference formula

$$\zeta_j R_i^n \left(\frac{w^{\,n}_{\,i+0.5,j} - w^{\,n}_{\,i-0.5,j}}{\Delta z} \right) - (\zeta_j)^2 \left(\frac{\partial R}{\partial z} \right)_i^n \left(\frac{w^{\,n}_{\,i,j+0.5} - w^{\,n}_{\,i,j-0.5}}{\Delta\zeta} \right) + \left(\frac{\zeta_{j+0.5} u^{\,n}_{\,i,j+0.5} - \zeta_{j-0.5} u^{\,n}_{\,i,j-0.5}}{\Delta\zeta} \right) = 0 \qquad (27)$$

The discretized form of the z-direction of the motion equation (17) becomes

$$\frac{w^{\,n+1}_{\,i+0.5,j} - w^{\,n}_{\,i+0.5,j}}{\Delta t} = \frac{\mathrm{P}^n_{i,j} - \mathrm{P}^n_{i+1,j}}{\Delta z} + \frac{\zeta_j}{R^n_{i+0.5}} \left(\frac{\partial R}{\partial z} \right)^n_{i+0.5} \left[\frac{\mathrm{P}^n_{i,j+1} + \mathrm{P}^n_{i+1,j+1} - \mathrm{P}^n_{i,j-1} - \mathrm{P}^n_{i+1,j-1}}{4\Delta\zeta} \right] + \mathrm{con} w^{\,n}_{\,i+0.5,j}$$
$$+ \frac{1}{\mathrm{Re}} (\mathrm{diff}\ w^{\,n}_{\,i+0.5,j} - M^2 w^{\,n}_{\,i+0.5,j}). \qquad (28)$$

In the same manner, the finite difference of the motion equation in the ζ -direction (18) is given by

$$\frac{u^{n+1}_{i,j+0.5} - u^n_{i,j+0.5}}{\Delta t} = \frac{1}{R^n_i} \left(\frac{\mathrm{P}^n_{\,i,j} - \mathrm{P}^n_{\,i,j+1}}{\Delta\zeta} \right) + \mathrm{con}\, u^n_{i,j+0.5} + \frac{1}{\mathrm{Re}} \left[\mathrm{diff}\ u^n_{i,j+0.5} \right] . \qquad (29)$$

The comprehensive numerical algorithm for the other model was already discussed elsewhere [28].

5. Numerical Results and Discussion

Figure-2 demonstrates the agreement with Haghighi *et al.* [9] on the axial velocity outcome at the stenostic region. The following parameter values were used for the numerical computations:
$\Delta\zeta = 0.0125,\ \Delta z = 0.1,\ Re = 300,\ \mathrm{z} = 14,\ L_0 = 10\ ,d = 7\ ,\ L = 30,\ U_0 = 0.5,\ \omega = 0.02, \tau_y = 0.$

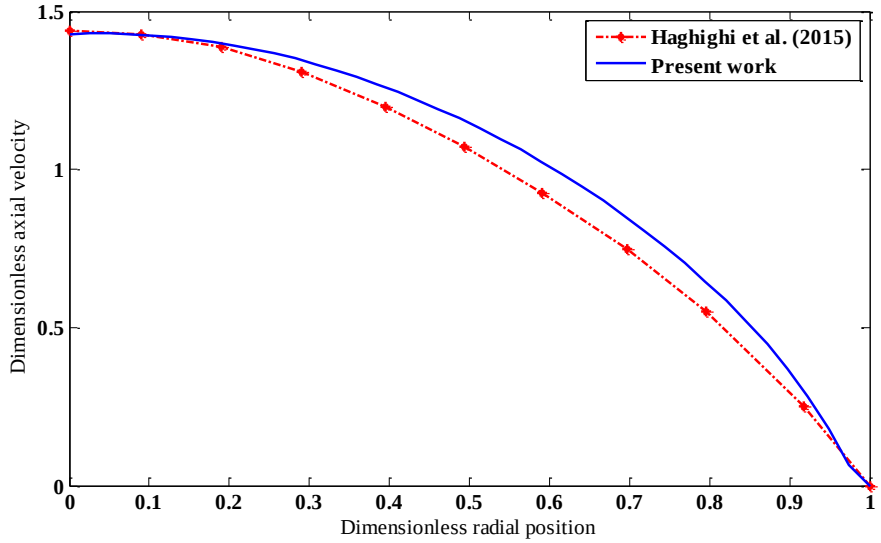

Figure 3-Dimensionless axial velocity profile

The graphical outcomes are displayed for the following parameters:

$Re = 300, d = 20, L_0 = 40, \delta_x = 0.5, L = 100, U_0 = 0.5, \omega = 0.02, \tau_y = 0.01$ and $\varepsilon_w = 0.858$.

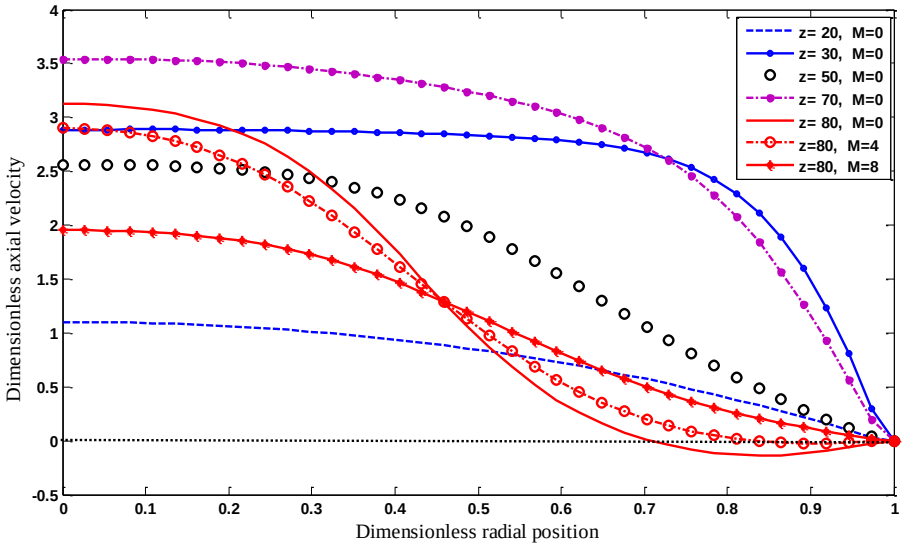

Figure 4-Velocity distribution for different values of *M* and for different axial locations

Figure-4 depicts the velocity profile for different values of Hartmann number and different axial locations. It is noted that the velocities decrease significantly with the increase in Hartmann number at the artery center. However, the velocity increases near the wall, which will help to prevent the backflow that occurs downstream the stenosis ($z = 80$) , which is determined when the velocity acquires a negative value also it is obviously observed, when M=0 and M=4 downstream the stenosis and terminate when M=8.

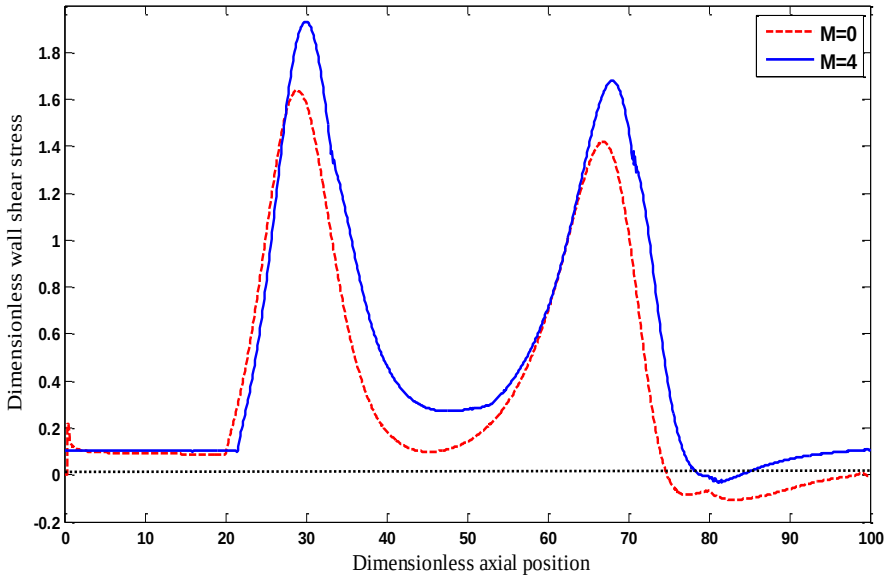

Figure 5- The variation of dimensionless wall shear stress with axial distance for different *M*

Figure-5 reveals that the wall shear stress increases substantially to reach its maximum height at the throats of the overlapping stenosis in the axial direction at z= 30 and z = 70. Also, it decreases from z = 80 to reach its minimum value downstream the stenosis in the axial direction, reaching minus values that indicate the backflow. It is also observed that the increase in *M* leads to an increase in the shear stress of the dimensionless wall.

Table-1 estimates dimensionless blood pressure across the first and second stenosis and along the artery with different values of Hartmann number *M* (magnetic intensity). It is noted that the value of pressure drop that occurs across the second stenosis is higher than that across the first one, reaching the highest value across the artery. Moreover, the pressure considerably increases with the increase of *M*.

Table 1-Diminsinless pressure drop across the overlapping stenosis

M	0	4	8
Presure across first stenosis	28.511	31.836	40.348
Presure across second stenosis	57.083	61.547	118.630
Presure across the artery	115.225	169.608	284.834

Figure-6 demonstrates the patterns of blood streamlines through the overlapping stenosis with various values of Hartmann number. It is obvious that more and larger recirculation zones develop at the downstream of the stenosis ($z = 80$) with M=0, while they diminish with M=4 and completely terminate when M=8.

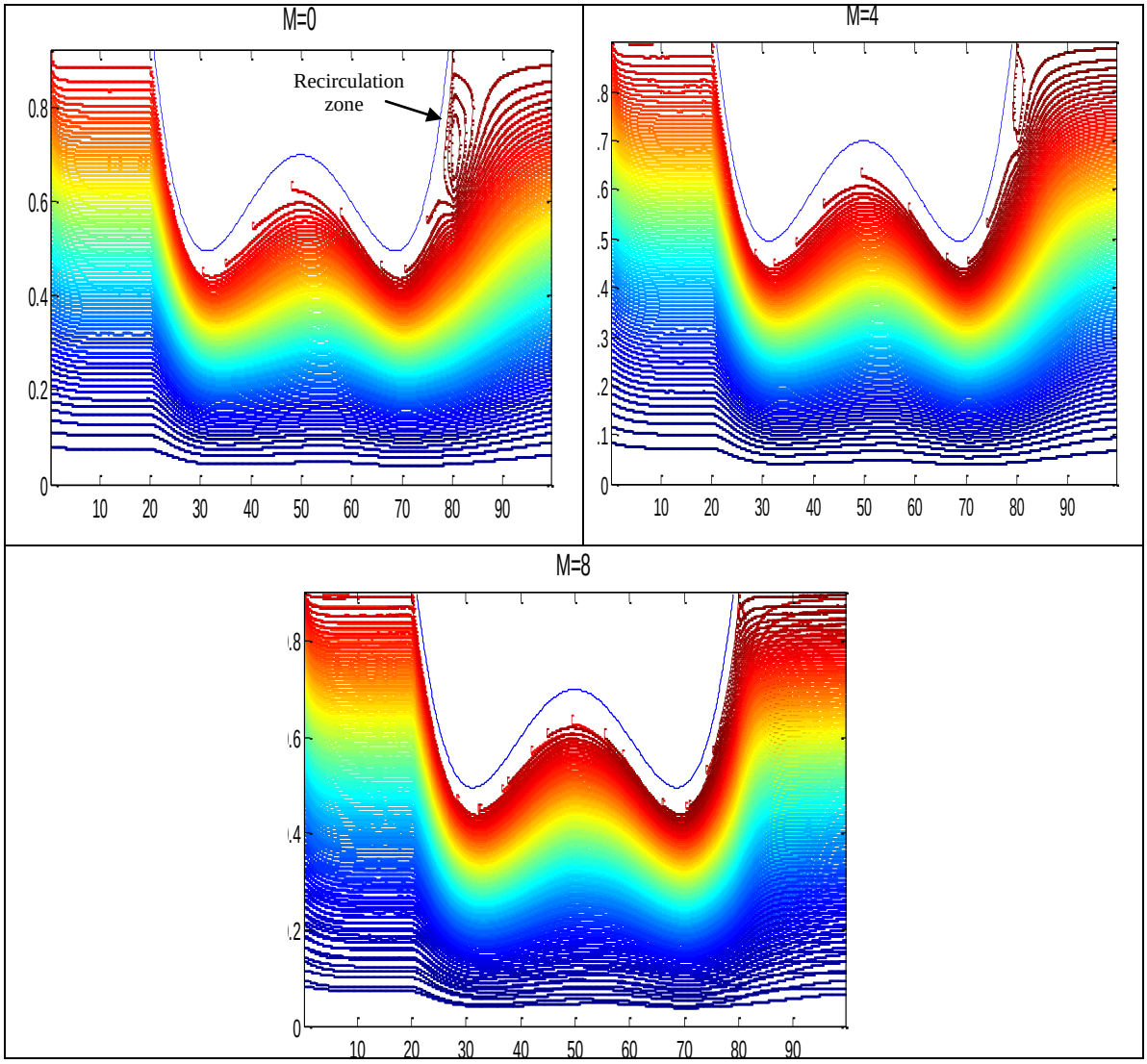

Figure 6-Streamline patterns for different values of M.

6. Conclusions

Blood flow is represented here by Casson model through an arterial segment having an overlapping stenosis. Significant outcomes revealed that both the magnetic intensity and the stenosis affect the characteristics of blood flow. Furthermore, the value of the pressure drops and the peak of the wall shear stress increases with the increase of magnetic intensity. On the other hand, for some specific value of magnetic intensity, blood recirculation zone can be diminished.

References

1. Onitilo, S., Usman, M. and Daniel, D. **2020**. Effects of Hematocrit on Blood Flow through a Stenosed Human Carotid Artery. *Iraqi Journal of Science*, 2106-2114.
2. Joshi, P., Pathak, A. and Joshi, B.K. **2009**. Two layered model of blood flow through composite stenosed artery, *Applications and Applied Mathematics*. **4(2)**: 343-354.
3. Srivastava, V. P. and Rastogi, R. **2010**. Blood flow through stenosed catheterized artery: effects of hematocrit and stenosis shape, *Computers & Mathematics with Applications*, **59**: 1377-1785.
4. Chakravarty, S. and Mandal, P. K. **1996**. A nonlinear two-dimensional model of blood flow in an overlapping arterial stenosis subjected to body acceleration, *Mathematical and Computer Modelling*, **24**: 43–58.
5. Chakravarty, S. and Mandal, P.K. **2000**. Two-dimensional blood flow through tapered arteries under stenotic conditions, *International Journal of Non-Linear Mechanics*, **35**: 779–793.

6. Ijaz, S., Iqbal, Z., Maraj, E. N. and Nadeem, S. **2018**. Investigation of Cu-CuO/blood mediated transportation in stenosed artery with unique features for theoretical outcomes of hemodynamics. *Journal of Molecular Liquids*, **254**: 421-432.

7. Chakravarty, S. and Mandal, P. K. **1994**. Mathematical modelling of blood flow through an overlapping arterial stenosis. *Mathematical and Computer Modelling*, **19**: 59-70.

8. Layek, G. Mukhopadhyay, C. S. and Gorla, R. S. D. **2009**. Unsteady viscous flow with variable viscosity in a vascular tube with an overlapping constriction, *International journal of engineering science*, **47**: 649-659.

9. Haghighi, A. R., Asl, M. S. and Kiyasatfar, M. **2015**. Mathematical modeling of micropolar fluid flow through an overlapping arterial stenosis, *International Journal of Biomathematics*, **8**(04): 1550056.

10. Mekheimer, K. S. and El Kot, M. A. **2012**. Mathematical modelling of unsteady flow of a Sisko fluid through an anisotropically tapered elastic arteries with time-variant overlapping stenosis, *Mathematical and Computer Modelling*, **36**(11): 5393-5407.

11. Srivastava, V. P. Mishra, S. and Rastogi, R. **2010**. Non-Newtonian arterial blood flow through an overlapping stenosis, *Applications and Applied Mathematic.*, **5**(1): 225-238.

12. Ismail, Z., Abdullah, I., Mustapha, N. and Amin, N. **2008**. A power-law model of blood flow through a tapered overlapping stenosed artery, *Mathematical and Computer Modelling***, 195**(2): 669-680.

13. Zaman, A., Ali, N. and Sajid, M. **2016**. Slip effects on unsteady non-Newtonian blood flow through an inclined catheterized overlapping stenotic artery, *Aip Advances*, **6**(1):015118.

14. Riahi, D. N., Roy, R. and Cavazos, S. **2011**. On arterial blood flow in the presence of an overlapping stenosis, *Mathematical and Computer Modelling*, **54**(11-12): 2999-3006.

15. Chakraborty, U. S. **2014**. Effect of slip on pulsatile flow of blood in a tube with an overlapping mild stenosis, *Journal of Biorheology*, **28**(1):21-28.

16. Zain, N. M. and Ismail, Z. **2017**. Modelling of Newtonian blood flow through a bifurcated artery with the presence of an overlapping stenosis, *Malaysian Journal of Fundamental and Applied Sciences.* **13**: 304-309.

17. Vijaya, R. B. **2017**. A mathematical model on Jeffrey fluid flow through an overlapping stenosis, *International Journal of Innovative Research in Science, Engineering and Technology*, **6**(13): 181-186.

18. Arunkumar, M. **2015**. Casson flow of blood through an arterial tube with overlapping stenosis, *IOSR J. Math.*, **11**(6): 26-30.

19. Prasad, K. M. Thulluri, S. and Phanikumari, M. V. **2017**. Investigation of blood flow through an artery in the presence of overlapping stenosis, *Journal of Naval Architecture and Marine Engineering*, **14**(1): 39-46.

20. Reddy, J. V.R. and Srikanth, D. **2015**.The polar fluid model for blood flow through a tapered artery with overlapping stenosis: effects of catheter and velocity slip, *Applied Bionics and Biomechanics*, **2015**:1-13.

21. Alnussairy, E. A., and Bakheet, A. **2019**. MHD Micropolar blood flow model through a multiple stenosed artery. In AIP Conference Proceedings, 2183(1), 090002. AIP Publishing.

22. Srivastava, V. P., Rastogi, R. and Vishnoi, R. 2010. A two-layered suspension blood flow through an overlapping stenosis, *Computers & Mathematics with Applications*, **60**(3): 432-441.

23. Srivastava, V. P., Vishnoi, R., Mishra, S. and Sinha, P. **2011**. A two-layered non-Newtonian arterial blood flow through an overlapping constriction, *AAM: Int. J.*, **6**(1): 41-57.

24. Srivastava, V. P., Vishnoi, R., Singh, D. and Mishra, S. **2015**. Response to blood flow through an overlapping stenosis in catheterized arteries, *e -Journal of Science & Technology* **5**: 93-103.

25. Sankar, D. S. and Viswanathan, K. K. **2019**. FDM analysis on pulsatile two-phase MHD rheology of blood in tapered stenotic blood vessels, *In Journal of Physics: Conference* Series, **1170**(1): 012002, IOP Publishing.

26. Hasen, S. S., and Abdulhadi, A.M. **2020**. MHD Effect on Peristaltic Transport for Rabinowitsch Fluid through A Porous Medium in Cilia Channel. *Iraqi Journal of Science*, 1461-1472.

27. Fung, Y.C. **1981**. *Biomechanics: Mechanical Properties of Living Tissues*, Springer, Berlin.

28. Bakheet, A., Alnussairy, E. A., and Ismail , Z. **2016**. Blood flow through an inclined stenosed artery. *Applied Mathematical Sciences***, 10**: 235-254.